Article

Unzipping of A-Form DNA-RNA, A-Form DNA-PNA, and B-Form DNA-DNA in the α-Hemolysin Nanopore

Rukshan T. Perera,[1] Aaron M. Fleming,[1] Amberlyn M. Peterson,[1] Jennifer M. Heemstra,[1] Cynthia J. Burrows,[1,*] and Henry S. White[1,*]
[1]Department of Chemistry, University of Utah, Salt Lake City, Utah

ABSTRACT Unzipping of double-stranded nucleic acids by an electric field applied across a wild-type α-hemolysin (αHL) nanopore provides structural information about different duplex forms. In this work, comparative studies on A-form DNA-RNA duplexes and B-form DNA-DNA duplexes with a single-stranded tail identified significant differences in the blockage current and the unzipping duration between the two helical forms. We observed that the B-form duplex blocks the channel 1.9 $\pm$ 0.2 pA more and unzips ~15-fold more slowly than an A-form duplex at 120 mV. We developed a model to describe the dependence of duplex unzipping on structure. We demonstrate that the wider A-form duplex (d = 2.4 nm) is unable to enter the vestibule opening of αHL on the *cis* side, leading to unzipping outside of the nanopore with higher residual current and faster unzipping times. In contrast, the smaller B-form duplexes (d = 2.0 nm) enter the vestibule of αHL, resulting in decreased current blockages and slower unzipping. We investigated the effects of varying the length of the single-stranded overhang, and studied A-form DNA-PNA duplexes to provide additional support for the proposed model. This study identifies key differences between A- and B-form duplex unzipping that will be important in the design of future probe-based methods for detecting DNA or RNA.

INTRODUCTION

Nanopores have found broad utility in a number of sensing applications (1–7). Protein-based nanopores harness the reproducibility of biological systems to furnish well-defined channels, some of which have high-resolution crystal structures to aid in understanding their properties (8,9). The most well studied is the α-hemolysin (αHL) nanopore, which has been applied to detect small molecules (8,10–12), proteins (13,14), carbohydrates (15), RNA (16,17), and predominantly DNA (18,19). Further, this protein channel also provides an excellent system for monitoring reactions (16,20) and conducting biophysical experiments to interrogate DNA secondary structures in solution (21–24). The size of the central constriction (d = 1.4 nm) allows single-stranded DNA (ssDNA; d = 1.0 nm), but not double-stranded DNA, to pass through the β-barrel (8,25). However, at higher voltages, the electric field along the pore is sufficient to unzip the duplex into single strands. After the first experimental demonstration of DNA unzipping by Sauer-Budge et al. (26), many studies have focused on utilizing duplex unzipping to detect metal ion binding (27), micro-RNA (28–30), and basepair mismatches (26,31,32).

Recently, our laboratory demonstrated that the latch zone of αHL can be used to differentiate a C•G basepair from an abasic site opposite G in duplex DNA when the duplex is temporarily immobilized in the channel (20,33). Immobilization is achieved through a single-stranded tail appended to one partner of the duplex to thread the molecules into the channel. Subsequent studies further optimized the latch-zone monitoring capabilities by adjusting the electrolyte concentration, cation identity, and the temperature (34,35).

The ~2.6 nm interior diameter of the latch allows smaller molecules to enter the vestibule while keeping larger ones outside when they are electrophoretically driven to the channel (8). For example, ssDNA and RNA (16,17), blunt-ended hairpins (36,37), fishhook hairpins (38), DNA-DNA duplexes (B-form duplexes) (26), small G-quadruplexes (24,39) and i-motif DNA (22) are able to enter the vestibule, but internal hairpins (38), large G-quadruplexes (24), and large proteins (37) cannot.

In this article, we report the use of an αHL nanopore to identify structural differences between A-form DNA-RNA or DNA-PNA and B-form DNA-DNA duplexes. The A-form duplex (d = 2.4 nm) (40–42) has a larger diameter than the B-form duplex (d = 2.0 nm) (25,42). The major differences between the A- and B-form duplex structures stem from the conformation of the sugar ring. In the B-form duplex, the sugar adopts the C2′ endo conformation, whereas the A-form has a C3′ endo conformation as a consequence of the 2′-OH in RNA. Moreover, the bases in A-form duplexes are displaced away from the central axis, resulting in a ribbon-like helical structure (40) with a wider core and larger diameter (Fig. 1 *C*).

In this study, we compared A- and B-form duplex unzipping in αHL by electrophoretically driving the anionic

Submitted August 31, 2015, and accepted for publication November 16, 2015.

*Correspondence: burrows@chem.utah.edu or white@chem.utah.edu

Editor: Hagan Bayley.

0006-3495/16/01/0306/9

http://dx.doi.org/10.1016/j.bpj.2015.11.020

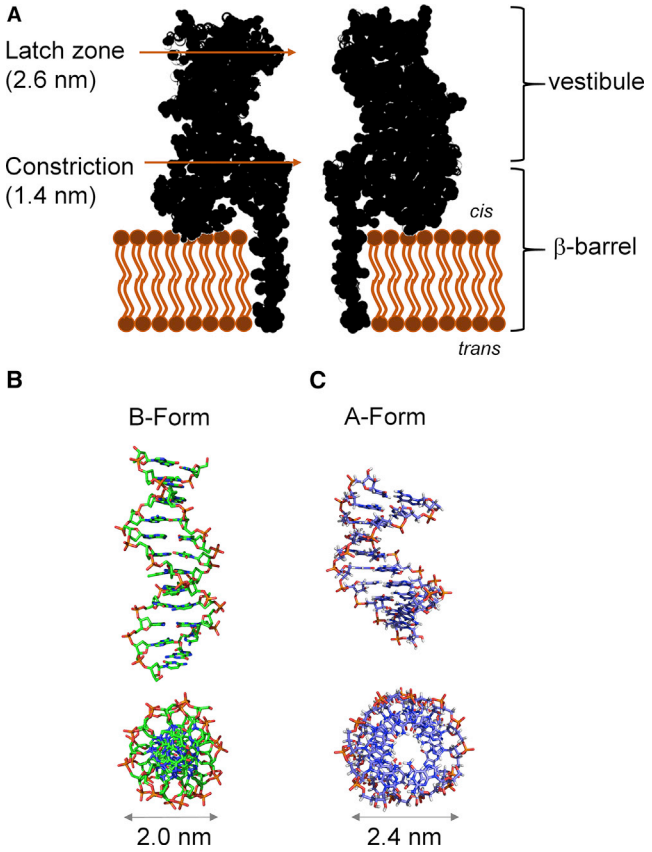

FIGURE 1 Structures for αHL and the duplex nucleic acids studied in this work. (*A*) Structure of wild-type αHL based on an x-ray crystal structure (PDB ID: 7AHL) (8). (*B*) Structure of a B-form DNA-DNA duplex (PDB ID: 1BNA) (25). (*C*) Structure of an A-form DNA-RNA duplex (PDB ID: 1RRR) (40). To see this figure in color, go online.

oligomers toward the nanopore. Lin et al. (43) previously reported RNA-RNA unzipping in αHL and the kinetics of helix to coil transformation of polyadenylic acid inside the β-barrel. Clamer et al. (44) also reported interactions between single-stranded RNA and the β-barrel. Therefore, for a better comparison of A- and B-form duplex unzipping, we chose to use the A-form helix of a DNA-RNA hybrid over an RNA-RNA duplex to eliminate possible interactions between the RNA overhang and the β-barrel. Duplexes without a single-stranded tail and with a 10- or 24-nucleotide (nt) tail attached to the 3′-end of one strand were probed, and comparisons of tail length versus unzipping of A- or B-form duplexes were made. Based on the work performed by Zhang et al. (28), it is assumed that the A-form DNA-RNA duplex enters the vestibule before it unzips. However, the data from our comparative studies support a model in which B-form duplexes enter the vestibule and unzip inside the nanopore, whereas the larger A-form DNA-RNA duplexes cannot enter the nanopore and therefore unzip on the outside. These features impose practical limitations for studying A-form duplexes inside the nanopore of wild-type αHL.

MATERIALS AND METHODS

DNA and RNA preparation

All DNA and RNA strands were synthesized from commercially available phosphoramidites (Glen Research, Sterling, VA) by the DNA/Peptide Core Facility at the University of Utah. The synthesized DNA oligomers were cleaved from the solid support and deprotected according to the manufacturer's protocol. Afterward, the DNA oligomers were purified by ion-exchange high-performance liquid chromatography using a previously described method (20). The PNA oligomers were synthesized on NovaSyn TGR R resin (0.2 mmol/g) using solid-phase peptide synthesis as described previously (45). The PNA strands were purified by reverse-phase high-performance liquid chromatography using a previously described method (46). The purification salts were removed by dialysis against double-distilled water (ddH_2O) for 36 h at 4°C, followed by concentration of the oligomers via lyophilization. The lyophilized samples were resuspended in ddH_2O and the concentrations were determined by the absorbance at 260 nm using the primary sequence to derive the extinction coefficient. All other chemicals were used without further purification.

Chemicals and materials

All electrolyte solutions contained 1 M KCl, 10 mM PBS, and 1 mM EDTA at pH 7.4. A conical-shaped nanopore in an ~50-μm-thick glass membrane at the end of the capillary was fabricated as previously described (47) and used to support the lipid bilayer (48). Before formation of the lipid bilayer, the glass surface was modified with 2% (v:v) 3-cyanopropyldimethylchlorosilane in CH_3CN for 6 h at room temperature to introduce a moderately hydrophobic surface. A solution of 1,2-diphytanoyl-*sn*-glycero-3-phosphochline dissolved in decane at 10 mg/mL was used to form the bilayer. Monomeric αHL purchased from List Biological Laboratories was diluted to a 1 mg/mL solution in ultrapure water (18 MΩ·cm) and stored at −80°C before use. DNA-DNA and DNA-RNA duplexes were formed by mixing them at a target/probe ratio of 1:4 to ensure complete hybridization, followed by annealing in a 90°C water bath for 3 min and cooling to room temperature over 2 h.

Ion-channel recordings

Current-time (*i-t*) recordings were performed using a custom-built high-impedance, low-noise system (Electronic Bio Sciences, San Diego, CA). The glass capillary and the reservoir were filled with the electrolyte solution. Two Ag/AgCl electrodes were placed in the solutions inside (*trans*) and outside (*cis*) of the capillary. The formation of a lipid bilayer across the glass nanopore membrane (GNM) was indicated by an increase in resistance from ~10 MΩ to ~100 GΩ. A gas-tight syringe was used to apply a pressure of 30–50 mmHg to the inside of the GNM capillary to facilitate protein insertion into the lipid bilayer (48). Heptameric wild-type αHL was reconstituted in the bilayer from the monomer peptide by adding 0.2 μL of a 1 mg/mL solution to the *cis* side (volume = 350 μL) of the GNM. The formation of a proper nanopore was determined by an I_o at 120 mV of 120 pA at 20°C. Nanopore measurements were performed at different applied voltages (*trans* versus *cis*), and data were recorded using a 10 kHz low-pass filter and a 50 kHz data acquisition rate. A K-type thermocouple was used to control the temperature with a precision of ±0.5°C.

Data analysis

We identified $i-t$ blockades longer than 500 μs as duplex unzipping events. Shorter events were assigned to translocation of the excess ssDNA present in the solution. A 4:1 mol ratio (longer strand versus shorter strand; see sequences below) was used to anneal the duplex and thus facilitate its formation. The current and duration of individual events were extracted using

QUB 2.0.0.29 software, and the data were analyzed using OriginPro 9.1. Density plots of blockade current versus duplex unzipping duration were generated using data analysis software provided by Electronic Bio Sciences. Histograms of the current amplitude were fitted by a Gaussian function, and the maximum of the distribution is reported for each duplex structure. The unzipping time τ was extracted by fitting the time histograms to an exponential decay and measuring the decay constant τ. The error values reported are standard errors for individual experiments. Unless otherwise stated, the representative data presented in each figure were obtained from a single experiment. However, each experiment was repeated at least three times. The residual current varied by only 0.2–0.4% between the different pores.

RESULTS AND DISCUSSION

Unzipping of DNA-DNA versus DNA-RNA duplexes

A- and B-form duplexes were driven into the αHL nanopore via an electrophoretic force to investigate their unzipping behavior. The representative A-form duplex consisted of one strand of DNA and one strand of RNA (DNA-RNA), and the representative B-form duplex was comprised of two DNA strands (DNA-DNA). The poly-C tail length was varied to be 0, 10, or 24 nt. Both duplexes had the same sequence, with the exception of U in RNA replaced by T in DNA.

DNA-RNA 5′-TCA TCA GTA GAA CTC AGA AAC TCC_n-3′ $n = 0$, 10, or 24
3′-AGU AGU CAU CUU GAG UCU UUG AG-5′
DNA-DNA 5′-TCA TCA GTA GAA CTC AGA AAC TCC_n-3′ $n = 0$, 10, or 24
3′-AGT AGT CAT CTT GAG TCT TTG AG-5′

Unzipping experiments were performed in solutions containing the DNA-DNA B-form duplex, the DNA-RNA A-form duplex, and a mixture of the A- and B-forms. A representative *i-t* trace for the mixture of A- and B-form duplexes is shown in Fig. 2 (data collected over 20 s for all three experiments are given in Figs. S1–S3 in the Supporting Material). Data collected in the presence of both A- and B-forms clearly identified significant differences between the unzipping times and blockage currents for the two helical forms, as demonstrated in Fig. 3 and discussed below.

A solution of the DNA-DNA B-form duplex studied at 120 mV (*trans* versus *cis*) gave a Gaussian-distributed histogram ($n = 433$) of blocking currents centered at 17.2 ± 0.1 pA (Fig. 3 *A*). Analysis of this population revealed an exponential distribution of unzipping times with a time constant (τ) of 390 ± 9 ms. The observed exponential time distribution was expected based on the first-order kinetic model for duplex unzipping (26), and consistent with previous studies (31,49,50). Next, a solution of the DNA-RNA A-form duplex, studied under identical conditions, showed a Gaussian-distributed histogram ($n = 794$) of blocking currents of 19.1 ± 0.2 pA (Fig. 3 *B*). A broader distribution of

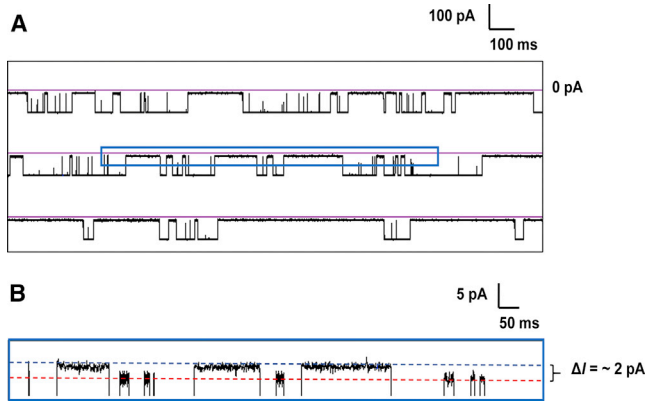

FIGURE 2 (*A*) Representative *i-t* trace showing uninterrupted data collected at 10 kHz at 120 mV. The mixture contained 8 μM of both A- and B-form duplexes with a 24-nt overhang in 1 M KCl, 10 mM PBS, pH 7.4 at 20°C. (*B*) The expanded window in (*A*) shows the deep-block-current differences between A- and B-form duplexes. The red dashed line represents the blocking current of A-form duplex and the blue dashed line indicates the blocking current of the B-form duplex during the unzipping process based on the individual experiments shown in Fig. 3, *A* and *B*. The expanded trace in (*B*) is filtered to 1 kHz for presentation purposes. To see this figure in color, go online.

blockage currents was observed for the DNA-RNA duplex unzipping, a consequence of the shorter timescale of analysis compared with the longer unzipping duration of the DNA-DNA duplex. Again, an exponential distribution of times was observed with $\tau = 25.9$ ± 0.6 ms. Voltage-dependent studies for both duplex systems demonstrated that the unzipping duration decreased with the applied voltage (Fig. S4), providing further evidence for unzipping (51,52). We also performed an unzipping experiment for DNA-RNA with a 40-nt overhang to investigate the dependence of unzipping kinetics on overhang lengths above 24-nt. (Fig. S5) The difference between the residual currents for the DNA-RNA with 24-nt and 40-nt overhangs is 0.4%, whereas the unzipping time differed only by 4.4 ± 2.1 ms. The results suggest that the longer overhang above 24-nt has a small effect on unzipping time or current blockage. Lastly, when both duplex systems were mixed together in an equimolar ratio, a histogram of blocking currents ($n = 652$) identified two Gaussian populations: one centered at 17 pA and the other centered at 19 pA (Fig. 3 *C*). The areas under the fitted Gaussian distributions were nearly identical (~295 and 269 events), which suggests that the capture frequency was independent of the duplex form, and is consistent with the capture frequency observed when each duplex was studied individually.

Comparisons of the A- and B-form duplex unzipping results identify critical differences in the unzipping times and blocking currents that at first glance appear to be counterintuitive. The larger A-form duplex gave a larger residual current (i.e., less blocking to the current) by 1.9 ± 0.2 pA compared with the smaller B-form duplex (Fig. 3 *C*). Additionally, previous studies have demonstrated that A-form

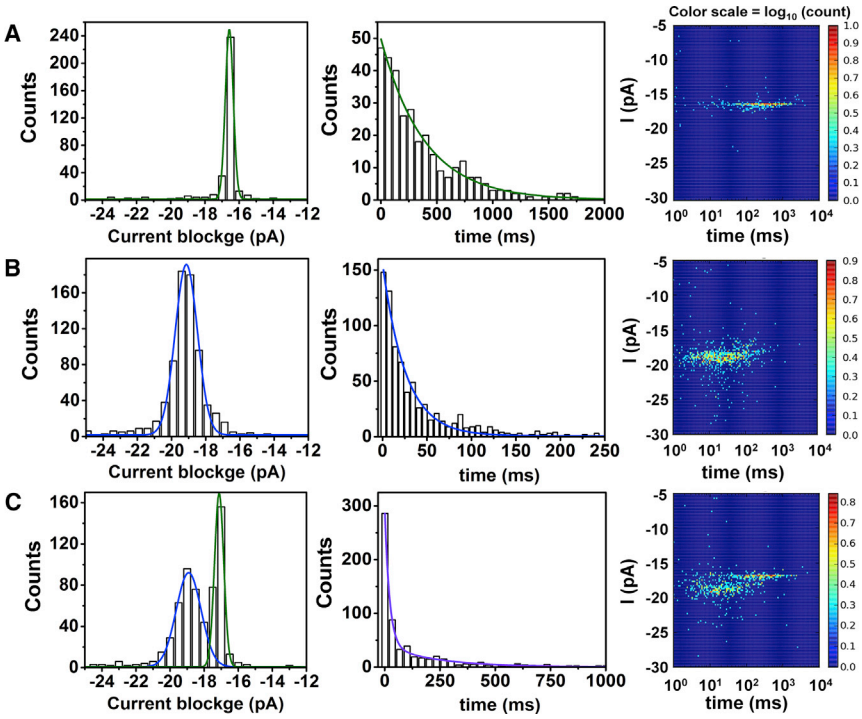

FIGURE 3 Current blockage, unzipping time duration, and *i-t* density plots for the duplex systems studied in this work. (*A–C*) DNA-DNA duplex (*A*, B-form), DNA-RNA duplex (*B*, A-form), and A- and B-form duplexes (*C*) were analyzed as a 1:1 mixture. All experiments were performed at 120 mV (*trans* versus *cis*) in 1 M KCl (10 mM PBS, pH 7.4) at 20°C in the presence of 8 μM of duplex. To see this figure in color, go online.

duplexes are generally more stable than B-form duplexes of the same sequences (53). This feature is determined by thermal melting experiments that identify the temperature (T_m) of the midpoint during the thermal denaturing process. A-form duplexes generally have T_m values that are 10–15°C above those measured for B-form duplexes with the same sequence (except for U in RNA and T in DNA) (54). For the electrolytes used here, the A-form duplex showed a T_m 10.5°C greater than the B-form duplex under the nanopore buffer and electrolyte conditions (Fig. S6). On the basis of these comparisons, we anticipated that the A-form duplex would exhibit the longer unzipping time. However, we observed the opposite: the A-form duplex displayed a 15-fold faster unzipping time than the B-form duplex (Fig. 3) at 120 mV.

In an attempt to understand these findings, we developed several models (Fig. 4). Smaller B-form duplexes pass through the latch zone and enter the vestibule, where they slowly unzip within the sterically confined protein cavity. In contrast, the wider A-form duplex cannot pass through the latch zone into the vestibule, and unzips outside the protein with fewer steric constraints inhibiting the unzipping process. Apart from the size of the structures, the conformational difference of the phosphate backbone between the A- and B-forms can change the hydration of the duplex (57). Several x-ray crystal and molecular-dynamics (MD) simulation studies have confirmed that the cations and water molecules are well ordered and less mobile in A-form compared with B-form duplexes (57–61). Therefore, we hypothesize that the stable systematic arrangement of solvent in the A-form can also create a barrier against entry into the nanopore. This model is also consistent with the notion that the smaller, less stable B-form duplex causes greater blockage to the open-channel current and has a longer unzipping time, whereas the wider, more stable A-form duplex is less blocking to the open-channel current and has a shorter unzipping time because only the single-stranded overhang enters the nanopore. This size-dependent model was

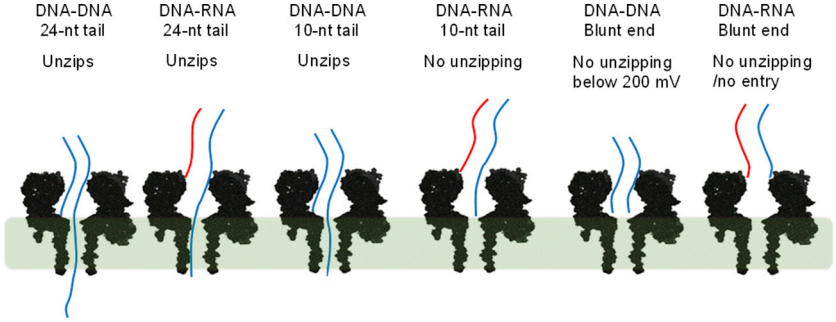

FIGURE 4 Proposed models for trapping and unzipping of DNA-RNA (A-form) and DNA-DNA (B-form) duplexes. The highlighted region shows the highest voltage drop across the pore based on both experiments and MD simulations (51,55,56). To see this figure in color, go online.

previously proposed based on studies performed in our laboratories, in which fishhook hairpins were observed to unzip more slowly than an internal hairpin (38). The internal hairpin cannot enter the vestibule and unzips outside the vestibule, giving rise to a faster unzipping (by 5- to 20-fold depending on the sequence) compared with the fishhook hairpin, which can be accommodated in the vestibule. The experiments described below provide additional support for this model.

The vestibule of αHL is ~5 nm long (8), and based on previous studies, this spans ~10 nt of ssDNA (55,62). Therefore, to test whether the A-form duplex was unzipping outside the nanopore, we decreased the tail length to 10 nt. An A-form duplex with a 10-nt tail will only lead to shallow current blockages because the tail cannot penetrate the central constriction of αHL. In contrast, a B-form duplex with a 10-nt tail should enter the vestibule, allowing the tail to pass the central constriction and fill the β-barrel, leading to deep blockages. Consistent with these predictions, the DNA-RNA A-form duplex with a 10-nt tail yielded shallow blockages (type 1) ($\%I/I_o$ ~50% ± 5%) and had residence times of <100 μs (Figs. 5 *A* and S7). Based on previous reports (17,63–65), the residual current observed indicates that the 10-nt overhang enters the vestibule, but does not pass the central constriction and cannot translocate through the pore. Interestingly, the event duration increased with increased voltage (Figs. 5 *C* and S8), and the absence of any deep-block-current level supports the proposal that the A-form duplex is held on the outside of the vestibule with the aid of the overhang before it eventually diffuses back to the bulk solution on the *cis* side.

On the other hand, the DNA-DNA B-form duplex yielded two event types (types 2 and 3) based on the *i-t* traces observed (Figs. 5 *B* and S9). The type 2 events showed deep blockages to the current ($\%I/I_o$ = 14% ± 1%) and the event time decreased as the voltage was increased (Fig. 5 *C*). These observations support the notion that the 10-nt tail enters the β-barrel before the duplex unzips. Type 3 events accounted for ~10% of the total events and gave residual currents at $\%I/I_o$ = 24% ± 1%, with stochastic spikes to $\%I/I_o$ = 10% ± 1%. The residual current, $\%I/I_o$ = 24% ± 1%, indicates that the duplex portion of the molecule enters the vestibule, but does not occupy the β-barrel (66). The spikes between 24 ± 1 pA and 10 ± 1 pA are due to the terminal nucleotides trying to enter the constriction zone and going back to the vestibule zone before exiting from the *cis* side of the nanopore when the polarity of the voltage is reversed. A similar observation was made in a previous analysis of blunt-ended B-form duplex interactions with the constriction zone inside the vestibule of αHL (36,37).

A second study with all blunt-ended A- and B-form duplexes provided additional support for our model. The DNA-RNA A-form duplex without a tail should not lead to any long-lived events, because it cannot pass through

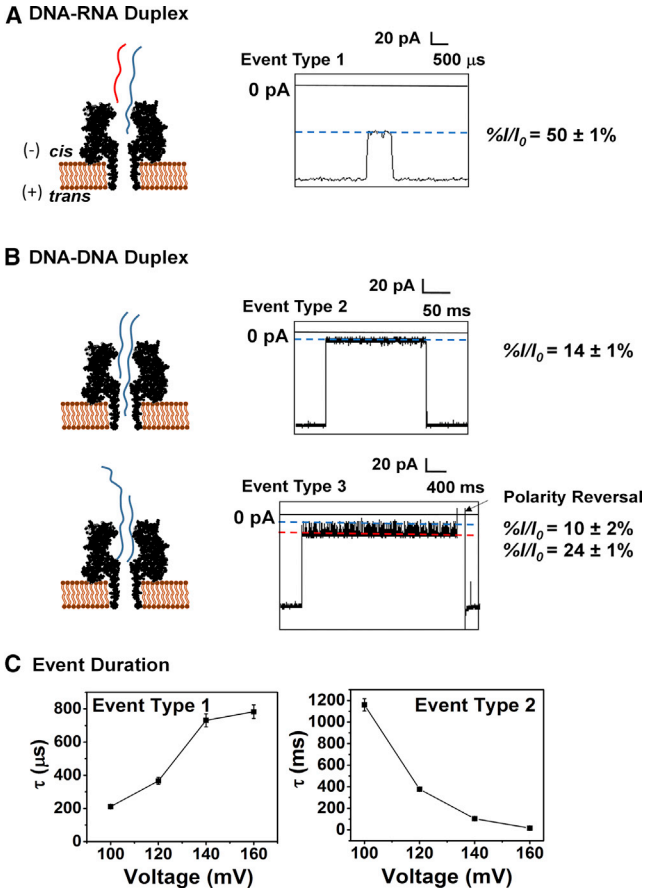

FIGURE 5 Studies for unzipping of A- and B-form duplexes with a shorter (10-nt) tail. (*A*) Unzipping of DNA-RNA. (*B*) DNA-DNA duplexes. All experiments were performed at 120 mV in 1 M KCl (10 mM PBS, pH 7.4) at 20°C. (*C*) Event durations for type 1 (*left*) and type 2 (*right*) were recorded at voltages of 100–160 mV. To see this figure in color, go online.

the opening of αHL. As anticipated, studies with this duplex at 80–200 mV did not give events with lifetimes of >500 μs (Figs. 6 *A* and S10). This observation supports the notion that the absence of the overhang prohibits entrance of the A-form duplex into the vestibule. The only *i-t* traces observed represented excess ssDNA with event times of <100 μs. This further verifies our model in which A-form duplexes cannot enter the vestibule.

The *i-t* traces corresponding to blunt-ended B-form duplexes yielded deep blockage currents with two distinct types of *i-t* patterns, termed types 3a and 3b (Figs. 6 *B* and S11). Both event types were long-lived and did not lead to unzipping events below 200 mV (Fig. S12). The type 3a events had residual currents of $\%I/I_o$ = 24% ± 1% (Fig. 6 *B*), a value we previously identified as the duplex inside the vestibule held up against the central constriction (Fig. 5 *B*) (51,66). The type 3b events gave residual currents of $\%I/I_o$ = 24% ± 1%, with current spikes to lower residual values of $\%I/I_o$ = 11% ± 1%. This *i-t* pattern is similar to that observed in previous studies (36,66) in which the deflections to lower currents were ascribed to the terminal

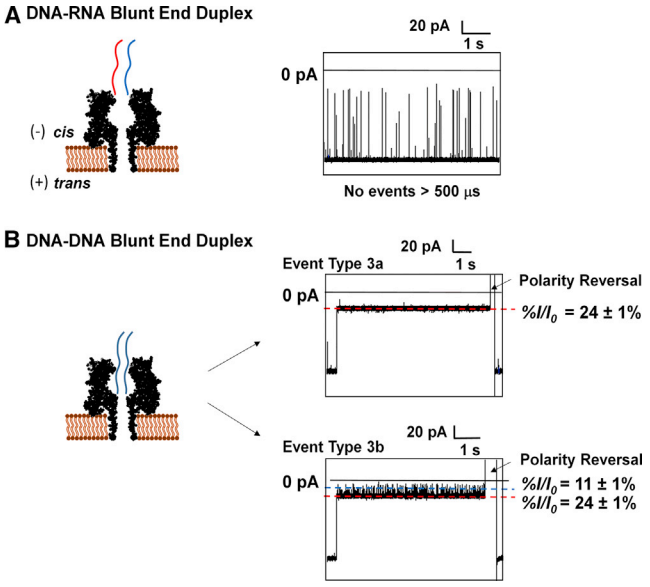

FIGURE 6 Unzipping of A- and B-form duplexes without a single-stranded tail. (*A* and *B*) Unzipping of (*A*) a DNA-RNA blunt-end duplex and (*B*) a DNA-DNA blunt-end duplex. All experiments were performed at 120 mV (*trans* versus *cis*) in 1 M KCl (10 mM PBS, pH 7.4) at 20°C. To see this figure in color, go online.

basepairs partially opening and interacting with the central constriction zone (Fig. 6 *B*). This can be further supported by the voltage-dependent frequency of fluctuations between the two current levels (Fig. S11). These tail-length-dependent studies provide further support for our hypothesis that A-form duplexes are incapable of passing through the mouth of the vestibule.

Both experimentally mapped (55) and MD simulation (56) results indicate that the voltage drop in the αHL nanopore occurs mainly at the β-barrel (~90%), as shown by the green highlighted zone in Fig. 4 (51). Because the DNA-DNA duplex can enter the vestibule, the highlighted region is fully occupied by both DNA-DNA duplexes having 10-nt and 24-nt overhangs (Fig. 4). Therefore, both duplexes are subjected to nearly the same amount of force (F = Eq, where F = electrophoretic force, E = electric field, and q = charge that is approximately proportional to the length of the overhang occupying the field). The unzipping durations for the two molecules are nearly the same (430 ms and 380 ms at 120 mV, respectively), further supporting the conclusion that both molecules are inside the vestibule during unzipping. However, the DNA-RNA duplex does not enter the vestibule, and only a duplex with a long overhang will penetrate deep enough into the pore where the force is great enough to unzip the duplex. In this study with the A-form duplex, a 24-nt overhang is long enough to occupy the β-barrel ($\%I/I_o = 14\% \pm 1\%$), experience the electric field, and unzip, whereas the 10-nt overhang only occupies the vestibule ($\%I/I_o = 50\% \pm 2\%$) and is not subject to sufficient electric force to unzip, and thus eventually diffuses away. The blunt-end DNA-DNA enters the vestibule ($\%I/I_o > 24\%$), whereas the blunt-end DNA-RNA duplex does not enter the vestibule, based on the blockage current, further validating our proposed model (Fig. 4).

In previous studies, we and others interrogated B-form duplex DNA when it was trapped inside the vestibule (20,33,34). On the basis of the results presented here, we concluded that similar experiments could not be performed with A-form duplexes. We next asked whether other biopolymers that form A-form helices also unzip outside the αHL pore. DNA-PNA duplexes adopt an A-form helix (67) and are more stable than DNA-DNA or DNA-RNA duplexes. Therefore, we analyzed the behavior of a DNA-PNA duplex with the αHL pore. Due to complications of synthesis and low solubility, we used a 10-bp-long PNA-DNA duplex (the sequence is given in Fig. S13). To our knowledge, this is the first time the unzipping behavior of a DNA-PNA duplex has been investigated. The *i-t* traces are shown in Fig. 7. Data collected over 20 s are given in Fig. S13 and the voltage dependence of the unzipping time is given in Fig. S14. The unzipping time observed for the DNA-PNA duplex is shown in Fig. 8. The observed unzipping time is of the same order of magnitude as the values observed for A-form DNA-RNA. Therefore, the data from this experiment provide residence times consistent with unzipping outside of the vestibule of αHL (Fig. 8).

The faster unzipping time of the A-form duplex compared with the B-form duplex further supports the proposal that A-form duplexes cannot enter the vestibule, and therefore unzipping occurs outside of the nanopore. To interrogate the significance of the orientation of the tail in unzipping, we also performed unzipping experiments with a 5′-poly C tail (24 nt). The unzipping times did not show any major difference (25.8 ms and 30.2 ms for 3′ and 5′ overhangs, respectively; for details see Fig. S15). Based on our studies, we conclude that the orientation of the overhang that enters the nanopore does not change the position of the duplex during the unzipping process. With the help of this systematic study, we demonstrate that the A-form DNA-RNA duplex cannot enter the vestibule, as assumed in previous studies performed by Zhang et al. (28), and the αHL nanopore can be used as a tool to identify the structural differences between A- and B-form duplexes.

The use of a probe-based approach to interrogate DNA and RNA has enormous potential for biotechnology

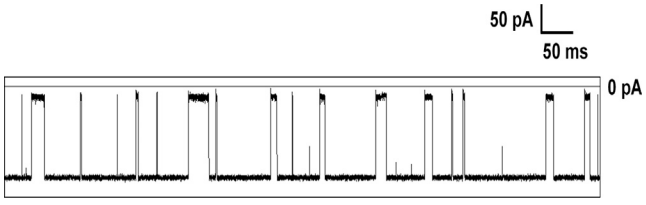

FIGURE 7 Sample *i-t* trace showing uninterrupted data collected at 10 kHz at 120 mV. The mixture contained 8 μM of DNA-PNA duplexes in 1 M KCl, 10 mM PBS, pH 7.4, at 20°C.

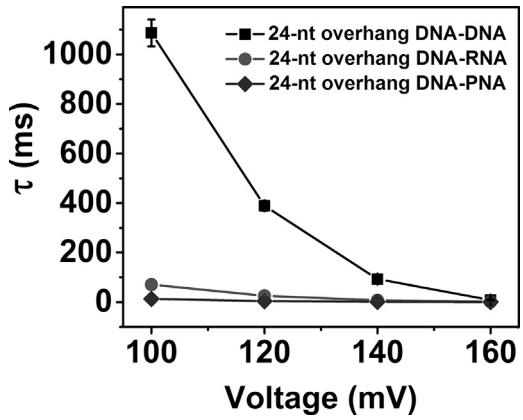

FIGURE 8 Unzipping duration as a function of voltage for DNA-DNA (*square*), DNA-RNA (*circle*), and DNA-PNA (*diamond*). The data were recorded at 20°C in 1 M KCl, 10 mM PBS, pH 7.4, and fit to an exponential decay equation to obtain the unzipping time.

applications (28–30). For example, DNA probes complementary to microRNAs (28,30) that are diagnostic of cancer progression have been detected and quantified with wild-type αHL. In probing experiments, the A-form DNA-RNA heteroduplexes were counted when a current deflection to the open-channel current was observed; however, the underlying details of the *i-t* traces were not deeply examined. Two recent studies by Wang et al. (51,68) highlighted the importance of understanding the unzipping process of DNA-RNA. Interestingly, neither of these studies actually used DNA-RNA duplexes; rather, they used DNA-DNA duplexes as a model. The model we have proposed for unzipping and trapping of the two different forms of the duplexes (A- and B-forms; Fig. 4) suggests practical limitations if studies are designed to interrogate A-form duplexes inside the vestibule of wild-type αHL. Because a high-resolution structure of this nanopore exists, site-directed mutagenesis may allow the engineering of new proteins with larger openings to the vestibule that can accommodate entry of A-form duplexes.

CONCLUSIONS

This study demonstrates that the structural differences between A- and B-form duplexes lead to different trapping, unzipping, and escaping processes during interactions with the wild-type αHL nanopore in an electric field (Fig. 4). These duplex-dependent differences in unzipping are described by a model in which the A-form duplexes do not enter the vestibule of wild-type αHL, leading to unzipping on the exterior of the nanopore. This unzipping process is characterized by a higher residual current and faster unzipping time. In contrast, B-form duplexes can enter the vestibule, where they unzip with a deeper block to the current and require a longer time to unzip. Further, the A-form DNA-PNA duplex unzips in a fashion similar to that observed for DNA-RNA. This work identifies key differences between the unzipping of A- and B-form duplexes in wild-type αHL that may prove to be critical in the design of probe-based methods utilizing this nanopore.

SUPPORTING MATERIAL

Fifteen figures are available at http://www.biophysj.org/biophysj/supplemental/S0006-3495(15)01177-7.

AUTHOR CONTRIBUTIONS

R.T.P., A.M.F., C.J.B., and H.S.W. designed the research. R.T.P. performed the ion-channel measurements. A.M.F. and A.M.P. synthesized and purified the oligomers. R.T.P., A.M.F., C.J.B., and H.S.W. wrote and edited the manuscript. J.M.H., C.J.B., and H.S.W. oversaw the research.

ACKNOWLEDGMENTS

We thank Dr. Robert P. Johnson, Dr. Eric Ervin, and Dr. Anna Schibel for helpful discussions. We also thank Electronic Bio Sciences Inc. (San Diego, CA) for donating the ion-channel recording instrument and software.

This work was supported by grants from the National Institutes of Health (R41 DA038989 and R01 GM093099) and the National Science Foundation (CHE 1308364 to J.M.H.). The oligonucleotides were provided by the DNA/Peptide Core Facility at the University of Utah, which is supported in part by the NCI Cancer Center (P30 CA042014).

REFERENCES

1. Deblois, R. W., and C. P. Bean. 1970. Counting and sizing of submicron particles by the resistive pulse technique. *Rev. Sci. Instrum.* 41: 909–916.
2. Ito, T., L. Sun, and R. M. Crooks. 2003. Simultaneous determination of the size and surface charge of individual nanoparticles using a carbon nanotube-based Coulter counter. *Anal. Chem.* 75:2399–2406.
3. Saleh, O. A., and L. L. Sohn. 2003. Direct detection of antibody-antigen binding using an on-chip artificial pore. *Proc. Natl. Acad. Sci. USA.* 100:820–824.
4. Bezrukov, S. M., and J. J. Kasianowicz. 1993. Current noise reveals protonation kinetics and number of ionizable sites in an open protein ion channel. *Phys. Rev. Lett.* 70:2352–2355.
5. Braha, O., B. Walker, …, H. Bayley. 1997. Designed protein pores as components for biosensors. *Chem. Biol.* 4:497–505.
6. Bezrukov, S. M., I. Vodyanoy, and V. A. Parsegian. 1994. Counting polymers moving through a single ion channel. *Nature.* 370:279–281.
7. Siwy, Z., D. Dobrev, …, K. Voss. 2003. Electro-responsive asymmetric nanopores in polyimide with stable ion-current signal. *Appl. Phys. A.* 76:781–785.
8. Song, L., M. R. Hobaugh, …, J. E. Gouaux. 1996. Structure of staphylococcal alpha-hemolysin, a heptameric transmembrane pore. *Science.* 274:1859–1866.
9. Yamashita, K., Y. Kawai, …, I. Tanaka. 2011. Crystal structure of the octameric pore of staphylococcal γ-hemolysin reveals the β-barrel pore formation mechanism by two components. *Proc. Natl. Acad. Sci. USA.* 108:17314–17319.
10. Gu, L. Q., O. Braha, …, H. Bayley. 1999. Stochastic sensing of organic analytes by a pore-forming protein containing a molecular adapter. *Nature.* 398:686–690.
11. Kasianowicz, J. J., D. L. Burden, …, H. Bayley. 1999. Genetically engineered metal ion binding sites on the outside of a channel's transmembrane beta-barrel. *Biophys. J.* 76:837–845.

12. Menestrina, G. 1986. Ionic channels formed by Staphylococcus aureus alpha-toxin: voltage-dependent inhibition by divalent and trivalent cations. *J. Membr. Biol.* 90:177–190.
13. Movileanu, L., J. P. Schmittschmitt, …, H. Bayley. 2005. Interactions of peptides with a protein pore. *Biophys. J.* 89:1030–1045.
14. Nivala, J., D. B. Marks, and M. Akeson. 2013. Unfoldase-mediated protein translocation through an α-hemolysin nanopore. *Nat. Biotechnol.* 31:247–250.
15. Kullman, L., M. Winterhalter, and S. M. Bezrukov. 2002. Transport of maltodextrins through maltoporin: a single-channel study. *Biophys. J.* 82:803–812.
16. Kasianowicz, J. J., E. Brandin, …, D. W. Deamer. 1996. Characterization of individual polynucleotide molecules using a membrane channel. *Proc. Natl. Acad. Sci. USA.* 93:13770–13773.
17. Akeson, M., D. Branton, …, D. W. Deamer. 1999. Microsecond time-scale discrimination among polycytidylic acid, polyadenylic acid, and polyuridylic acid as homopolymers or as segments within single RNA molecules. *Biophys. J.* 77:3227–3233.
18. Henrickson, S. E., M. Misakian, …, J. J. Kasianowicz. 2000. Driven DNA transport into an asymmetric nanometer-scale pore. *Phys. Rev. Lett.* 85:3057–3060.
19. Meller, A., L. Nivon, and D. Branton. 2001. Voltage-driven DNA translocations through a nanopore. *Phys. Rev. Lett.* 86:3435–3438.
20. Jin, Q., A. M. Fleming, …, H. S. White. 2013. Base-excision repair activity of uracil-DNA glycosylase monitored using the latch zone of α-hemolysin. *J. Am. Chem. Soc.* 135:19347–19353.
21. Shim, J. W., Q. Tan, and L. Q. Gu. 2009. Single-molecule detection of folding and unfolding of the G-quadruplex aptamer in a nanopore nanocavity. *Nucleic Acids Res.* 37:972–982.
22. Ding, Y., A. M. Fleming, …, C. J. Burrows. 2015. Unfolding kinetics of the human telomere i-motif under a 10 pN force imposed by the α-hemolysin nanopore identify transient folded-state lifetimes at physiological pH. *J. Am. Chem. Soc.* 137:9053–9060.
23. An, N., A. M. Fleming, …, C. J. Burrows. 2015. Nanopore detection of 8-oxoguanine in the human telomere repeat sequence. *ACS Nano.* 9:4296–4307.
24. An, N., A. M. Fleming, …, C. J. Burrows. 2014. Single-molecule investigation of G-quadruplex folds of the human telomere sequence in a protein nanocavity. *Proc. Natl. Acad. Sci. USA.* 111:14325–14331.
25. Drew, H. R., R. M. Wing, …, R. E. Dickerson. 1981. Structure of a B-DNA dodecamer: conformation and dynamics. *Proc. Natl. Acad. Sci. USA.* 78:2179–2183.
26. Sauer-Budge, A. F., J. A. Nyamwanda, …, D. Branton. 2003. Unzipping kinetics of double-stranded DNA in a nanopore. *Phys. Rev. Lett.* 90:238101.
27. Wang, Y., B.-Q. Luan, …, L.-Q. Gu. 2014. Single molecule investigation of Ag+ interactions with single cytosine-, methylcytosine- and hydroxymethylcytosine-cytosine mismatches in a nanopore. *Sci. Rep.* 4:5883.
28. Zhang, X., Y. Wang, …, L. Q. Gu. 2014. Programming nanopore ion flow for encoded multiplex microRNA detection. *ACS Nano.* 8:3444–3450.
29. Tian, K., Z. He, …, L. Q. Gu. 2013. Designing a polycationic probe for simultaneous enrichment and detection of microRNAs in a nanopore. *ACS Nano.* 7:3962–3969.
30. Wang, Y., D. Zheng, …, L. Q. Gu. 2011. Nanopore-based detection of circulating microRNAs in lung cancer patients. *Nat. Nanotechnol.* 6:668–674.
31. Schibel, A. E. P., A. M. Fleming, …, C. J. Burrows. 2011. Sequence-specific single-molecule analysis of 8-oxo-7,8-dihydroguanine lesions in DNA based on unzipping kinetics of complementary probes in ion channel recordings. *J. Am. Chem. Soc.* 133:14778–14784.
32. Sutherland, T. C., M. J. Dinsmore, …, J. S. Lee. 2004. An analysis of mismatched duplex DNA unzipping through a bacterial nanopore. *Biochem. Cell Biol.* 82:407–412.
33. Jin, Q., A. M. Fleming, …, H. S. White. 2013. Structural destabilization of DNA duplexes containing single-base lesions investigated by nanopore measurements. *Biochemistry.* 52:7870–7877.
34. Johnson, R. P., A. M. Fleming, …, H. S. White. 2014. Effect of an electrolyte cation on detecting DNA damage with the latch constriction of α-hemolysin. *J. Phys. Chem. Lett.* 5:3781–3786.
35. Johnson, R. P., A. M. Fleming, …, H. S. White. 2014. Temperature and electrolyte optimization of the α-hemolysin latch sensing zone for detection of base modification in double-stranded DNA. *Biophys. J.* 107:924–931.
36. Vercoutere, W. A., S. Winters-Hilt, …, M. Akeson. 2003. Discrimination among individual Watson-Crick basepairs at the termini of single DNA hairpin molecules. *Nucleic Acids Res.* 31:1311–1318.
37. Winters-Hilt, S., W. Vercoutere, …, D. Haussler. 2003. Highly accurate classification of Watson-Crick basepairs on termini of single DNA molecules. *Biophys. J.* 84:967–976.
38. Ding, Y., A. M. Fleming, …, C. J. Burrows. 2014. Internal vs fishhook hairpin DNA: unzipping locations and mechanisms in the α-hemolysin nanopore. *J. Phys. Chem. B.* 118:12873–12882.
39. Shim, J. W., and L.-Q. Gu. 2008. Encapsulating a single G-quadruplex aptamer in a protein nanocavity. *J. Phys. Chem. B.* 112:8354–8360.
40. Gyi, J. I., A. N. Lane, …, T. Brown. 1998. Solution structures of DNA.RNA hybrids with purine-rich and pyrimidine-rich strands: comparison with the homologous DNA and RNA duplexes. *Biochemistry.* 37:73–80.
41. Wang, A. H. J., S. Fujii, …, A. Rich. 1982. Molecular structure of r(GCG)d(TATACGC): a DNA-RNA hybrid helix joined to double helical DNA. *Nature.* 299:601–604.
42. Arias-Gonzalez, J. R. 2014. Single-molecule portrait of DNA and RNA double helices. *Integr Biol (Camb).* 6:904–925.
43. Lin, J., A. Kolomeisky, and A. Meller. 2010. Helix-coil kinetics of individual polyadenylic acid molecules in a protein channel. *Phys. Rev. Lett.* 104:158101.
44. Clamer, M., L. Höfler, …, H. Bayley. 2014. Detection of 3′-end RNA uridylation with a protein nanopore. *ACS Nano.* 8:1364–1374.
45. Joshi, R., D. Jha, …, J. Engelmann. 2011. Facile synthesis of peptide nucleic acids and peptide nucleic acid-peptide conjugates on an automated peptide synthesizer. *J. Pept. Sci.* 17:8–13.
46. De Costa, N. T. S., and J. M. Heemstra. 2013. Evaluating the effect of ionic strength on duplex stability for PNA having negatively or positively charged side chains. *PLoS One.* 8:e58670.
47. Zhang, B., J. Galusha, …, H. S. White. 2007. Bench-top method for fabricating glass-sealed nanodisk electrodes, glass nanopore electrodes, and glass nanopore membranes of controlled size. *Anal. Chem.* 79:4778–4787.
48. White, R. J., E. N. Ervin, …, H. S. White. 2007. Single ion-channel recordings using glass nanopore membranes. *J. Am. Chem. Soc.* 129:11766–11775.
49. Jin, Q., A. M. Fleming, …, H. S. White. 2012. Unzipping kinetics of duplex DNA containing oxidized lesions in an α-hemolysin nanopore. *J. Am. Chem. Soc.* 134:11006–11011.
50. Nakane, J., M. Wiggin, and A. Marziali. 2004. A nanosensor for transmembrane capture and identification of single nucleic acid molecules. *Biophys. J.* 87:615–621.
51. Wang, Y., K. Tian, …, L. Q. Gu. 2014. Probing molecular pathways for DNA orientational trapping, unzipping and translocation in nanopores by using a tunable overhang sensor. *Nanoscale.* 6:11372–11379.
52. Dudko, O. K., J. Mathé, …, G. Hummer. 2007. Extracting kinetics from single-molecule force spectroscopy: nanopore unzipping of DNA hairpins. *Biophys. J.* 92:4188–4195.
53. Casey, J., and N. Davidson. 1977. Rates of formation and thermal stabilities of RNA:DNA and DNA:DNA duplexes at high concentrations of formamide. *Nucleic Acids Res.* 4:1539–1552.
54. Roberts, R. W., and D. M. Crothers. 1992. Stability and properties of double and triple helices: dramatic effects of RNA or DNA backbone composition. *Science.* 258:1463–1466.

55. Howorka, S., and H. Bayley. 2002. Probing distance and electrical potential within a protein pore with tethered DNA. *Biophys. J.* 83:3202–3210.

56. Aksimentiev, A., and K. Schulten. 2005. Imaging alpha-hemolysin with molecular dynamics: ionic conductance, osmotic permeability, and the electrostatic potential map. *Biophys. J.* 88:3745–3761.

57. Hud, N. V., and M. Polak. 2001. DNA-cation interactions: the major and minor grooves are flexible ionophores. *Curr. Opin. Struct. Biol.* 11:293–301.

58. Feig, M., and B. M. Pettitt. 1999. Sodium and chlorine ions as part of the DNA solvation shell. *Biophys. J.* 77:1769–1781.

59. McConnell, K. J., and D. L. Beveridge. 2000. DNA structure: what's in charge? *J. Mol. Biol.* 304:803–820.

60. Soler-López, M., L. Malinina, …, J. A. Subirana. 1999. Water and ions in a high resolution structure of B-DNA. *J. Biol. Chem.* 274:23683–23686.

61. Auffinger, P., and E. Westhof. 2001. Water and ion binding around r(UpA)12 and d(TpA)12 oligomers—comparison with RNA and DNA (CpG)12 duplexes. *J. Mol. Biol.* 305:1057–1072.

62. Stoddart, D., A. J. Heron, …, H. Bayley. 2009. Single-nucleotide discrimination in immobilized DNA oligonucleotides with a biological nanopore. *Proc. Natl. Acad. Sci. USA.* 106:7702–7707.

63. Deamer, D. W., and D. Branton. 2002. Characterization of nucleic acids by nanopore analysis. *Acc. Chem. Res.* 35:817–825.

64. Mathé, J., A. Aksimentiev, …, A. Meller. 2005. Orientation discrimination of single-stranded DNA inside the α-hemolysin membrane channel. *Proc. Natl. Acad. Sci. USA.* 102:12377–12382.

65. Vercoutere, W., S. Winters-Hilt, …, M. Akeson. 2001. Rapid discrimination among individual DNA hairpin molecules at single-nucleotide resolution using an ion channel. *Nat. Biotechnol.* 19:248–252.

66. Liu, A., Q. Zhao, …, X. Guan. 2011. Unzipping of double-stranded DNA in engineered α-hemolysin pores. *J. Phys. Chem. Lett.* 2:1372–1376.

67. Wittung, P., P. E. Nielsen, …, B. Nordén. 1994. DNA-like double helix formed by peptide nucleic acid. *Nature.* 368:561–563.

68. Wang, X., Y. Li, …, H.-C. Wu. 2015. The effect of secondary structures on the generation of characteristic events during the translocation of DNA hybrid through α-hemolysin. *Sci. China Chem.* Published online July 23, 2015. http://dx.doi.org/10.1007/s11426-015-5455-1.

Supporting Information

Unzipping of A-Form DNA-RNA, A-Form DNA-PNA, and B-Form DNA-DNA in the α-Hemolysin Nanopore

Rukshan T. Perera,[1] Aaron M. Fleming,[1] Amberlyn M. Peterson,[1] Jennifer M. Heemstra,[1] Cynthia J. Burrows,[1,*] and Henry S. White[1,*]

[1]Department of Chemistry, University of Utah, Salt Lake City, Utah

*To whom correspondence should be addressed.

E-mail: burrows@chem.utah.edu or white@chem.utah.edu

Contents

1. Sample *i-t* trace of a mixture containing B-form duplex.

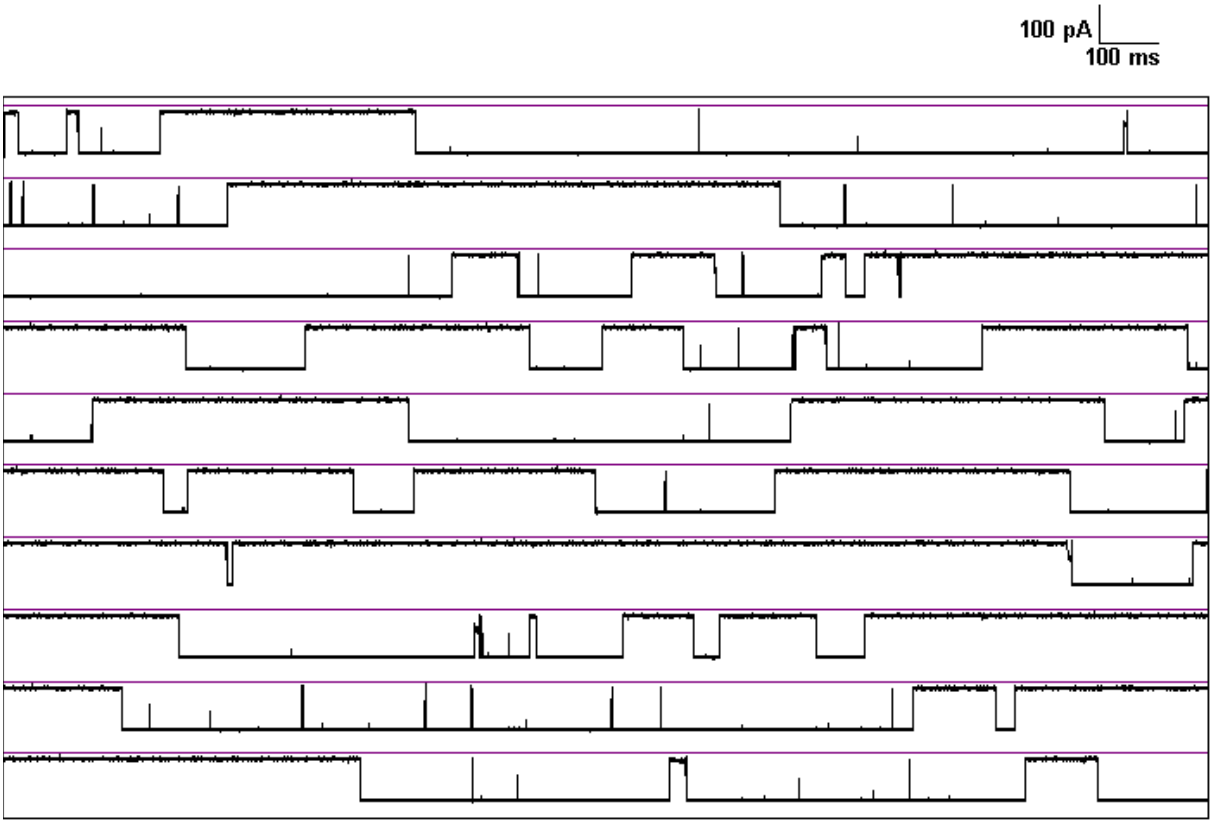

Figure SI1. A sample *i-t* trace showing uninterrupted data collected at 10 kHz for 20 s at 120 mV. The mixture contained 8 μM B-form duplex in 1 M KCl, 10 mM PBS, pH 7.4 at 20 °C.

2. Sample *i-t* trace of a mixture containing A-form duplex.

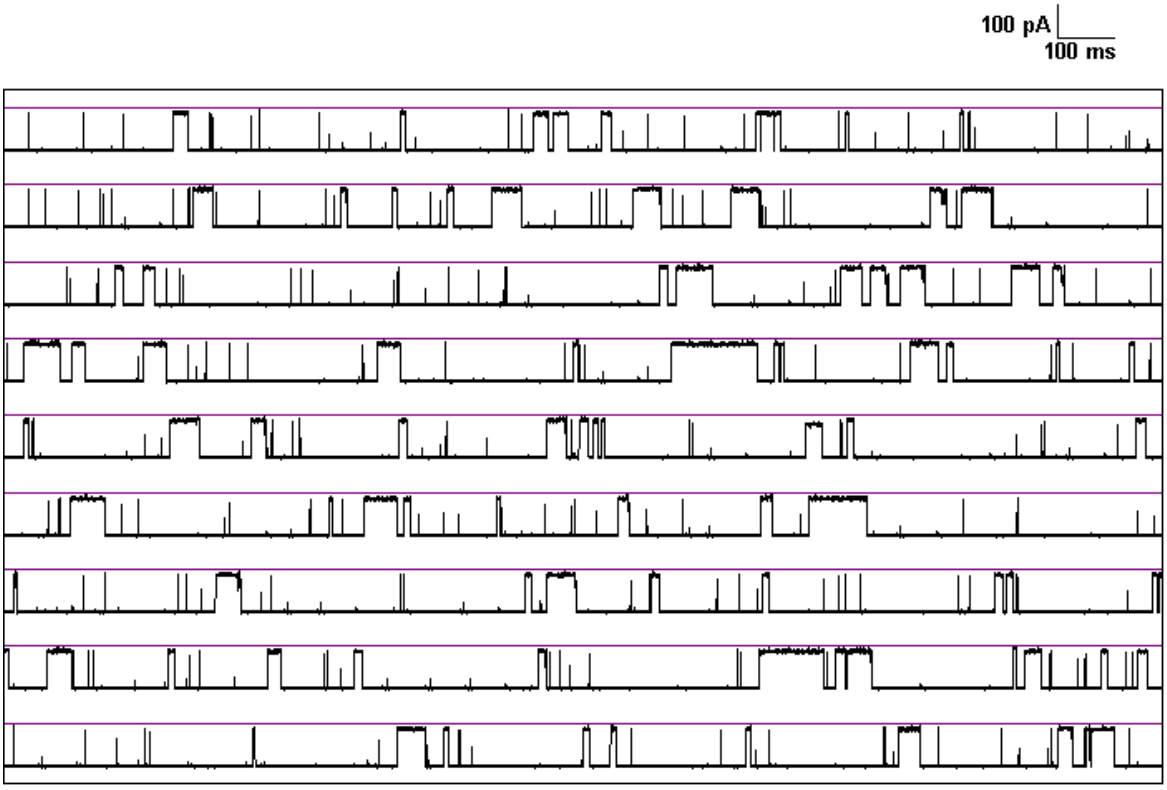

Figure SI2. A sample *i-t* trace showing uninterrupted data collected at 10 kHz for 20 s at 120 mV. The mixture contained 8 μM A-form duplex in 1 M KCl, 10 mM PBS, pH 7.4 at 20 °C.

3. Sample *i-t* trace of a mixture containing both A- and B-form.

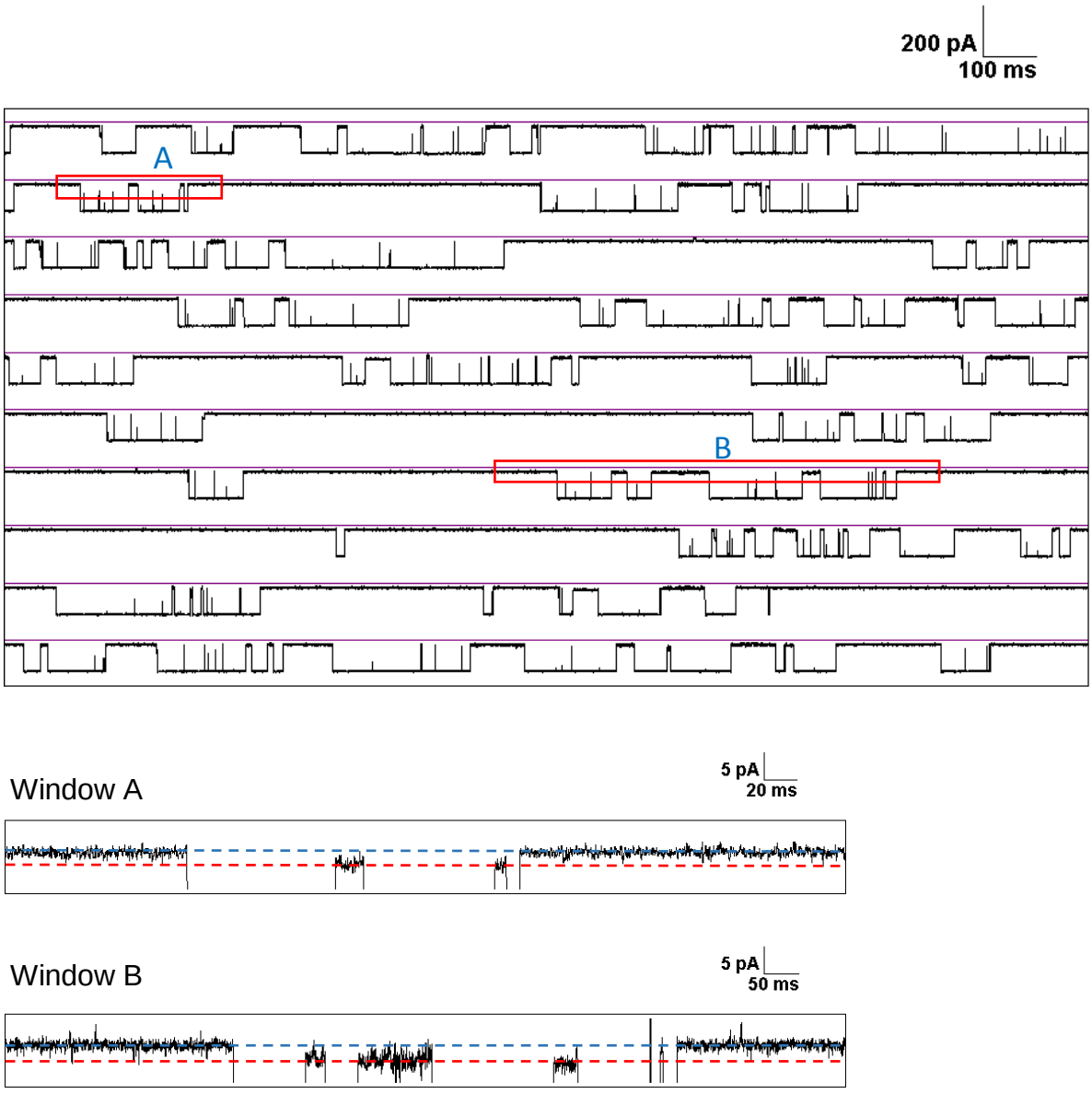

Figure SI3. A sample *i-t* trace showing uninterrupted data collected at 10 kHz for 20 s at 120 mV. The mixture contained 8 μM A- and B-form duplexes in 1 M KCl, 10 mM PBS, pH 7.4 at 20 °C. The two expanded windows, A and B, show the deep block current differences between A- and B-form duplexes. The expanded area is filtered to 1 kHz for presentation purpose.

4. Voltage dependence of unzipping times for DNA-RNA and DNA-DNA duplexes

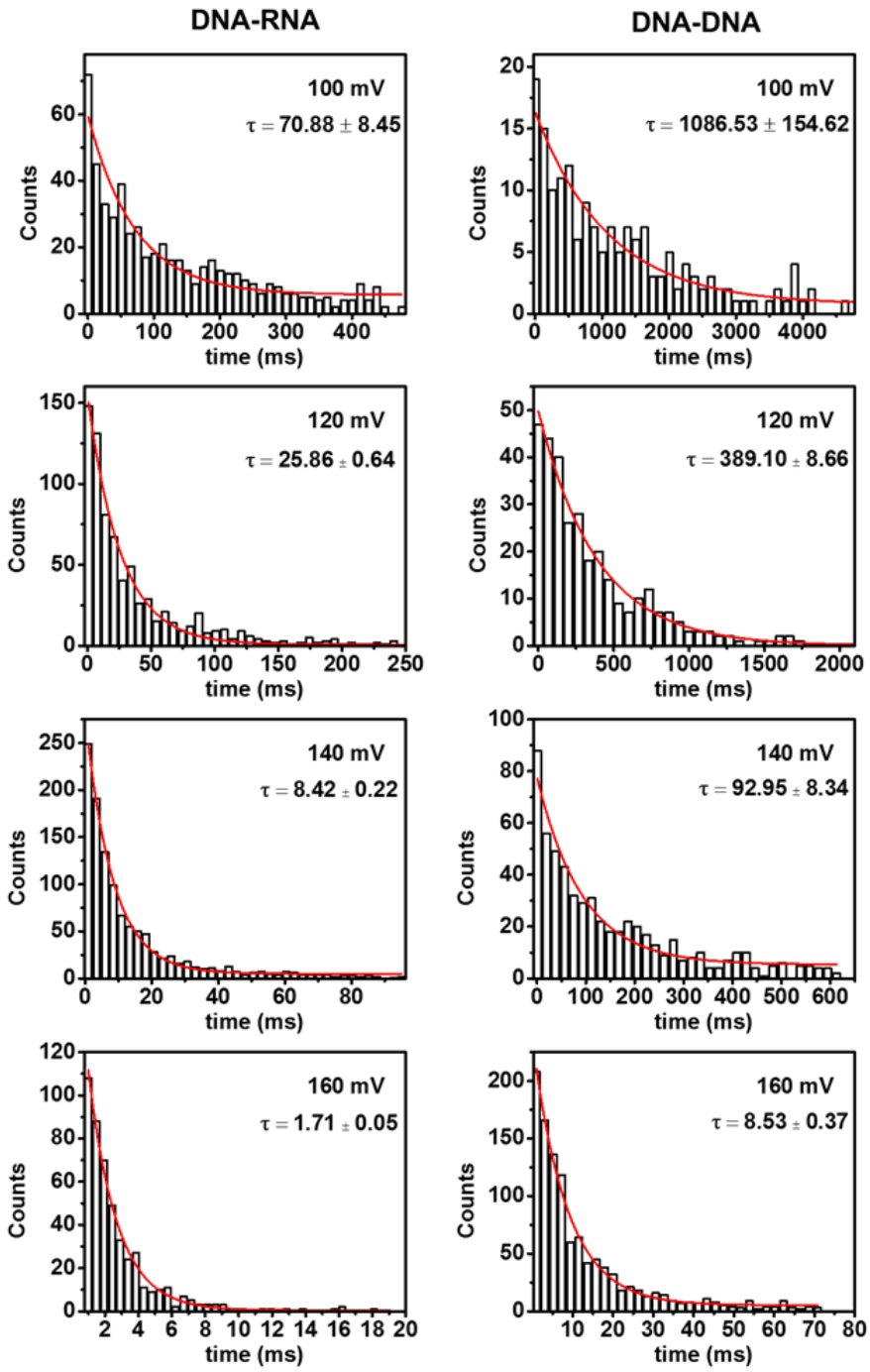

Figure SI4. Unzipping duration histograms as a function of voltage for DNA-RNA (left) and DNA-DNA (right) duplexes. The data were recorded at 20 °C in 1 M KCl, 10 mM PBS, pH 7.4. An exponential decay was fit to the data to obtain the unzipping time.

5. Unzipping of DNA-RNA duplex with 40-nt overhang.

Sequence of DNA-RNA duplex with 40–nt overhang.

DNA-RNA 5`-TCA TCA GTA GAA CTC AGA AAC $TCC_n$-3` n = 40

3`-AGU AGU CAU CUU GAG UCU UUG AG-5`

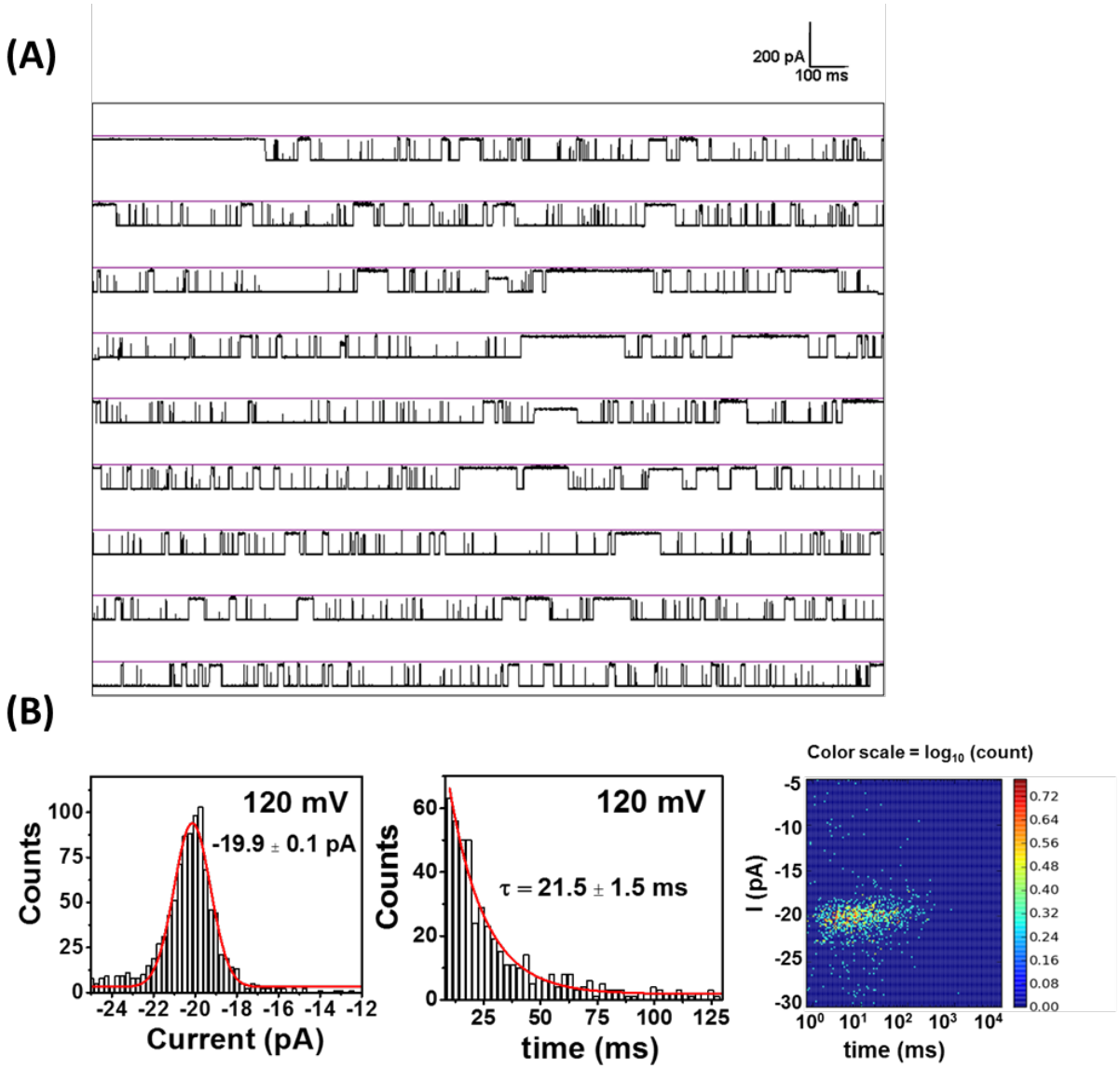

Figure SI5. (*A*) A sample *i-t* trace showing uninterrupted data collected at 10 kHz for 20 s at 120 mV. The mixture contained 10 μM DNA-RNA duplex with 40-nt overhang in 1 M KCl, 10 mM PBS, pH 7.4 at 20 °C. (*B*) Current blockage, unzipping time duration, and *i-t* density plots for DNA-RNA duplex with 40–nt overhang.

6. Thermal melting analysis of A-and B-form duplexes.

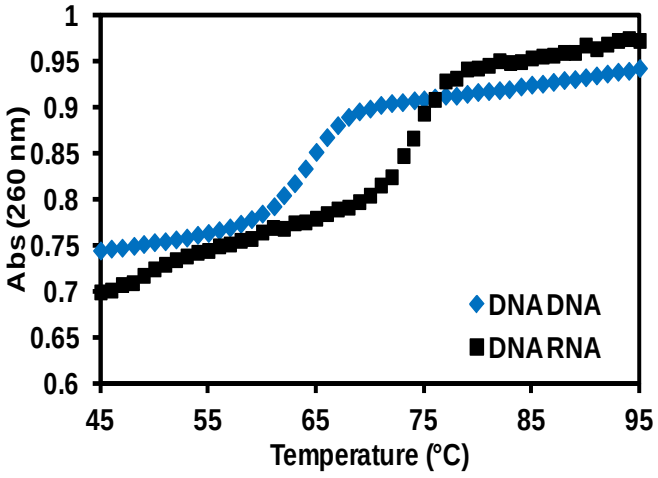

Sequences
DNA-DNA Duplex 5`-TCA TCA GTA GAA CTC AGA AAC TC-3` 3`-AGT AGT CAT CTT GAG TCT TTG AG-5`
DNA-RNA Duplex 5`-TCA TCA GTA GAA CTC AGA AAC TC-3` 3'-AGU AGU CAU CUU GAG UCU UUG AG-5`

Figure SI6. Thermal melting analysis of the DNA-DNA and DNA-RNA duplexes. All measurements were performed in 10 mM PBS, pH 7.4. The absorbance at 260 nm, $Abs_{260\ nm}$, was monitored as the temperature was increased from 20 °C to 100 °C at a ramp rate of 1 °C/min. At each time interval, the temperature was equilibrated for 30 s prior to making each absorbance measurement. Each experiment was conducted in triplicate.

7. Continuous *i-t* trace of DNA-RNA duplex with 10-nt overhang at 160 mV.

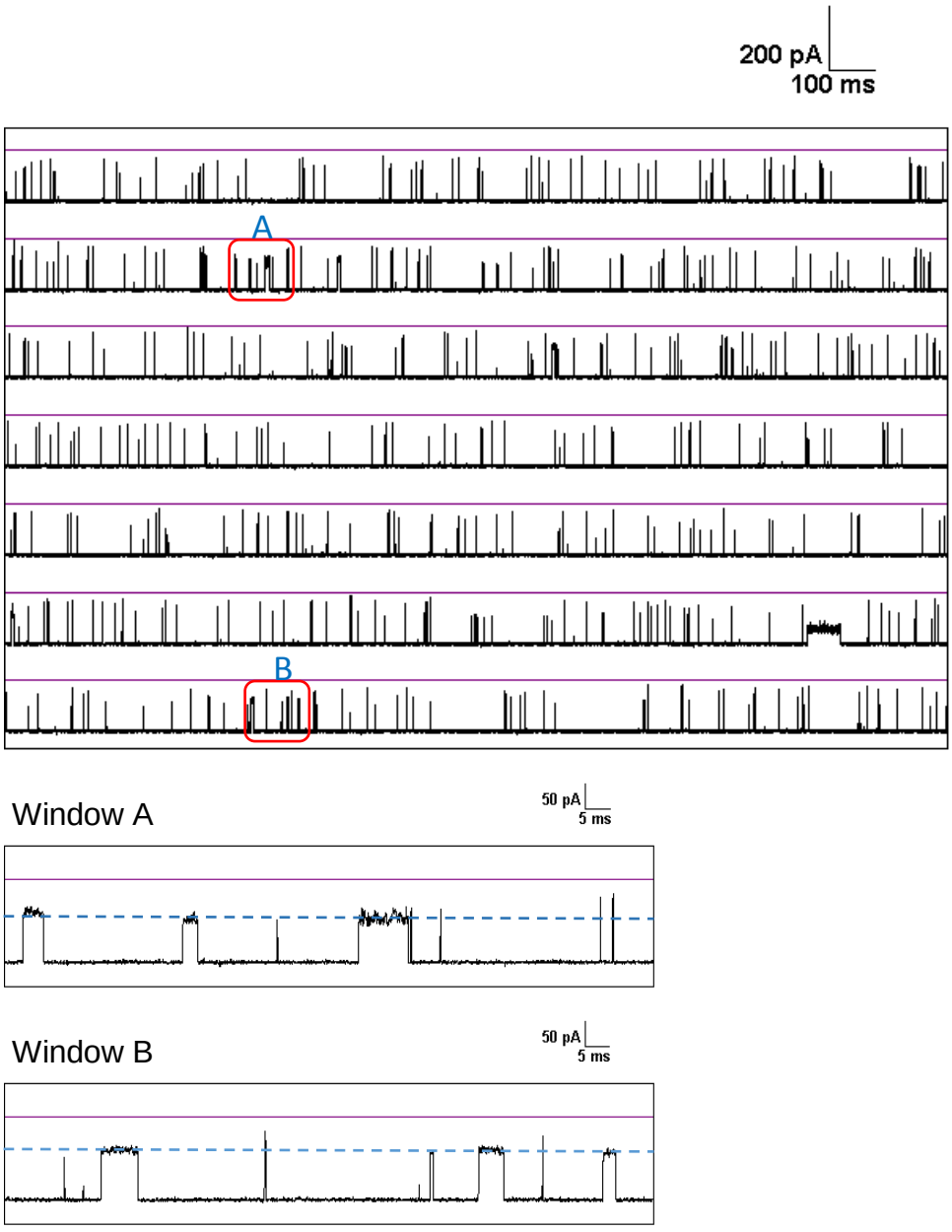

Figure SI7. A sample *i-t* trace showing uninterrupted data collection at 10 kHz for 20 s at 120 mV. The mixture contained 8 μM of DNA-RNA duplex with 10-nt overhang in 1 M KCl, 10 mM PBS, pH 7.4 at 20 °C. The two expanded windows (A and B) show the blockage due to occupation of the 10-nt overhang in the vestibule.

8. Voltage dependent trapping time of the DNA-RNA duplex with 10-nt overhang.

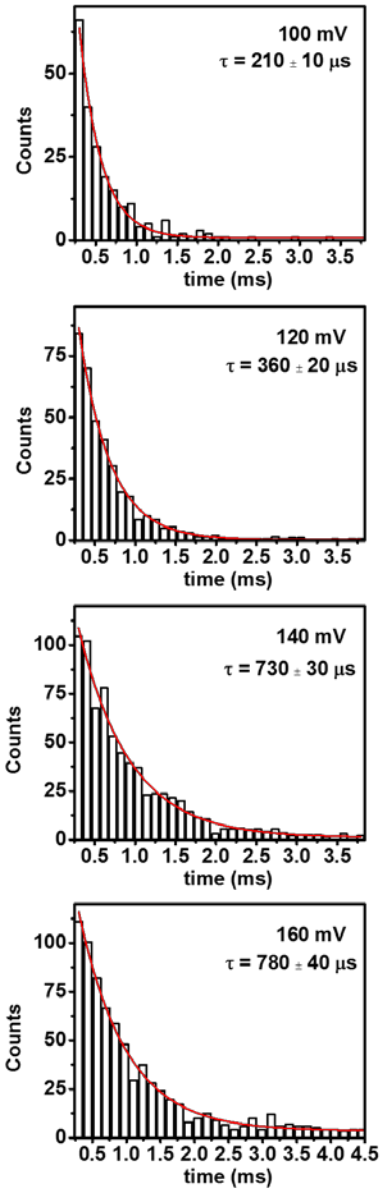

Figure SI8. Trapping time duration histograms as a function of voltage for DNA-RNA duplex with a 10-nt overhang. Only the events with $\%I/I_o$ between 20 and 80 and $\tau >$ 200 μs were analyzed as duplex unzipping events (single strand translocation is much faster). Data were recorded at 20 °C in 1 M KCl, 10 mM PBS, pH 7.4. An exponential decay was fit to the data to obtain the unzipping time.

9. Sample *i-t* trace of DNA-DNA duplex with 10-nt overhang at 160 mV.

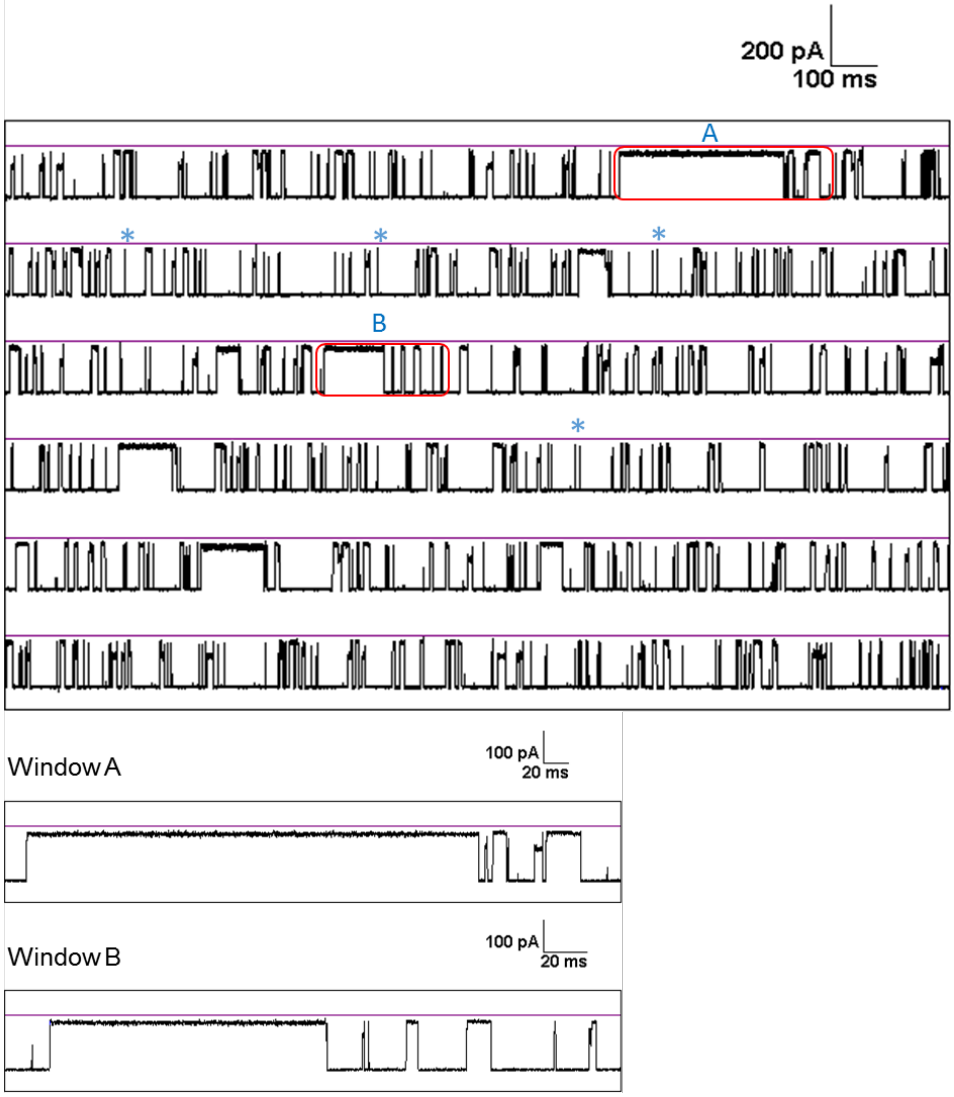

Figure SI9. A sample *i-t* trace showing uninterrupted data collection at 10 kHz for 20 s at 160 mV. The mixture contained 8 μM of the DNA-DNA duplex with 10-nt overhang in 1 M KCl, 10 mM PBS, pH 7.4 at 20 °C. The two expanded windows (A and B) show long-current blocks are due to unzipping of the duplex and the shorter blocks (less than 1 ms denoted by asterisks) are from translocation of the excess ssDNA.

10. Sample *i-t* trace of DNA-RNA duplex with no overhang.

Figure SI10. A continuous *i-t* trace showing uninterrupted data collection at 10 kHz for 20 s at 160 mV. The mixture contained 8 μM DNA-RNA blunt end duplex in 1 M KCl, 10 mM PBS, pH 7.4 at 20 °C. The expanded window A shows short translocation events (less than 500 μs) that are due to excess single strands present in the mixture.

11. Sample *i-t* trace of DNA-DNA duplex with no overhang.

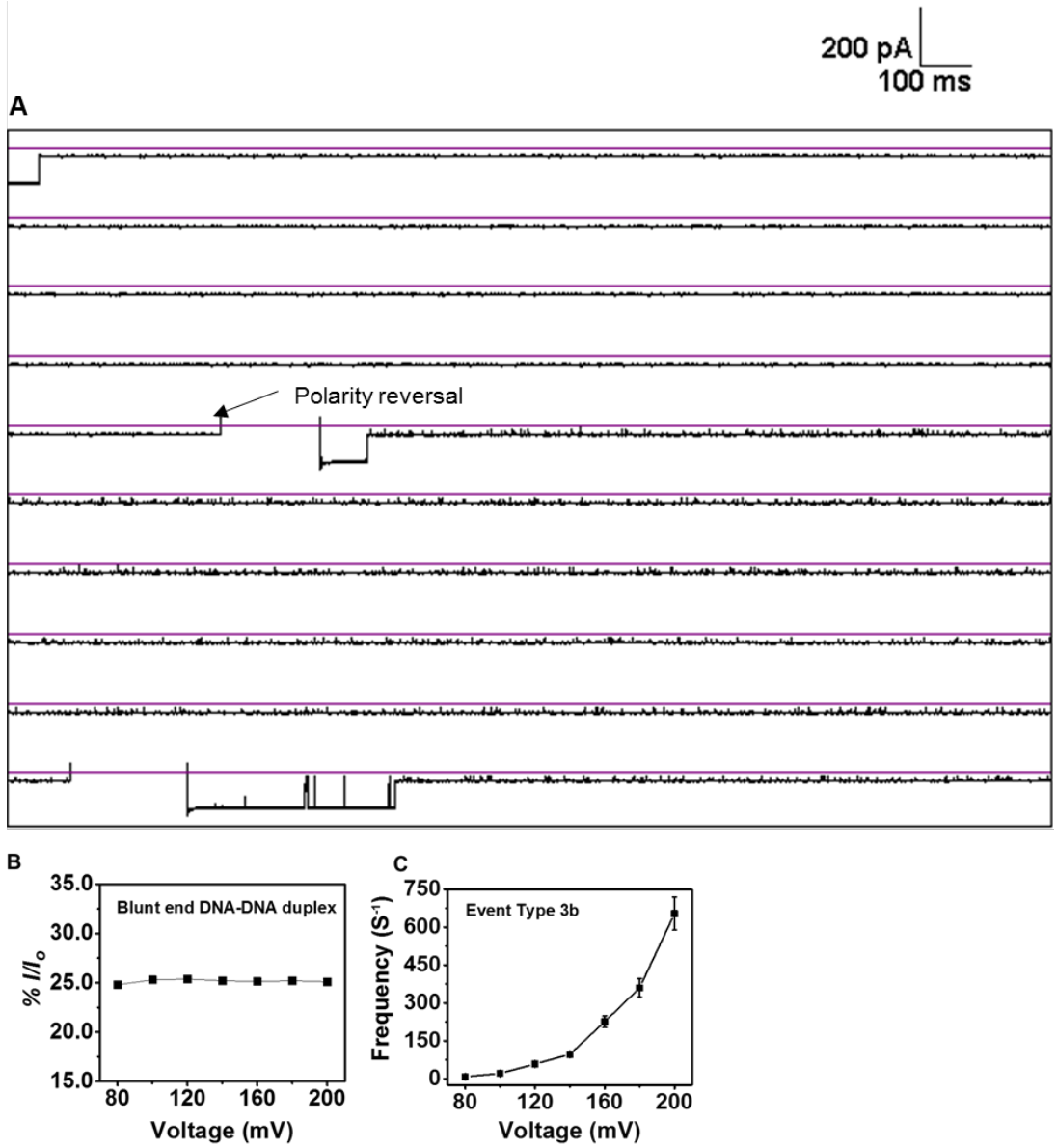

Figure SI11. (*A*) A continuous *i-t* trace showing uninterrupted data collection at 10 kHz for 10 s at 120 mV. The *cis* side contained 8 μM DNA-DNA blunt end duplex in 1 M KCl, 10 mM PBS, pH 7.4 at 20 °C. Long-current blockages show the duplex occupying the vestibule and the short events (less than 1 ms) are due to translocation of excess single strands. Interruption of the current blockage was due to the polarity reversal of the channel to remove the duplex in the nanopore. (*B*) Residual current when a blunt end duplex is inside the vestibule as a function of voltage. (*C*) Frequency of the events between two current levels shown in Event Type 3b in the main text Fig. 5B.

12. Sample *i-t* trace of DNA-DNA duplex with no overhang at 200 mV.

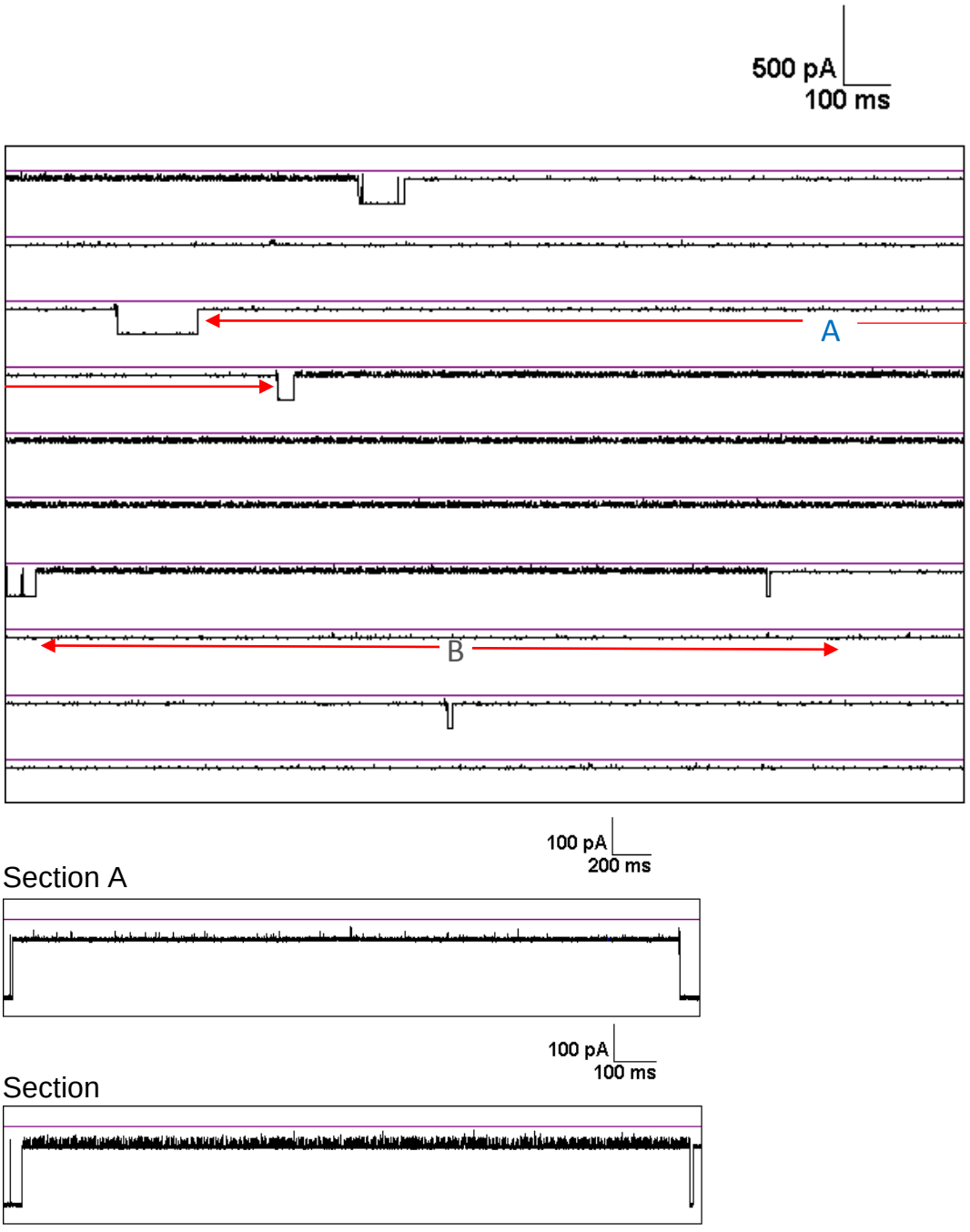

Figure SI12. A sample *i-t* trace showing uninterrupted data collection at 10 kHz for 20 s at 200 mV. The blunt end duplex unzips at 200 mV but not at 120 mV (see preceding section). The mixture contained 8 μM of the DNA-DNA duplex with 10-nt overhang in 1 M KCl, 10 mM PBS, pH 7.4 at 20 °C. The two expanded windows (A and B) shows long-current blocks are due to unzipping of the duplex.

13. Sample *i-t* trace of a mixture containing DNA-PNA duplex.

Sequence of DNA-PNA duplex

DNA-PNA 5`-N GTA GAT CAC T-Lys -3`

3`-CAT CTA GTG $A_{24}$-5`

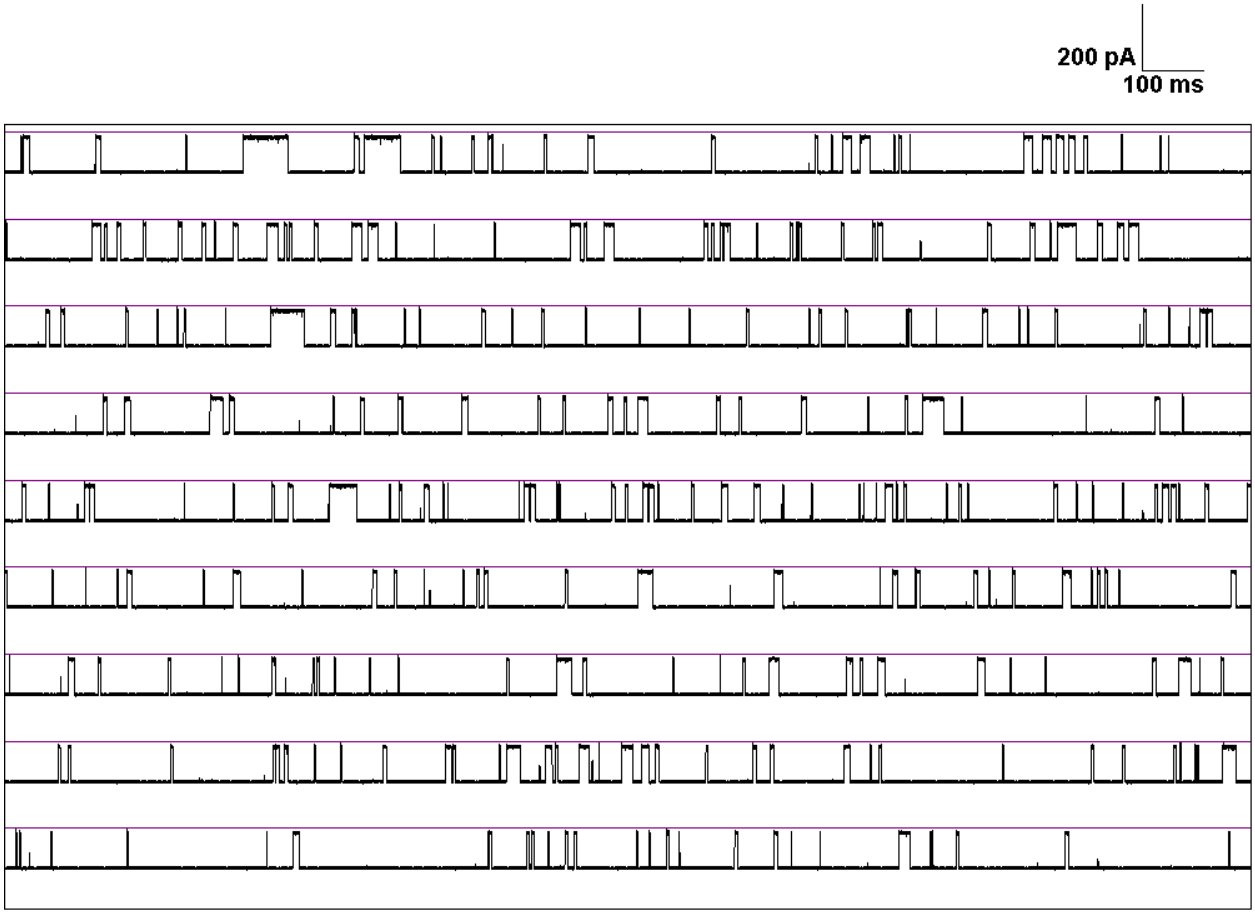

Figure SI13. A sample *i-t* trace showing uninterrupted data collected at 10 kHz for 20 s at 120 mV. The mixture contained 8 μM DNA-PNA duplex in 1 M KCl, 10 mM PBS, pH 7.4 at 20 °C.

14. Unzipping time and voltage dependent unzipping for DNA-PNA duplexes.

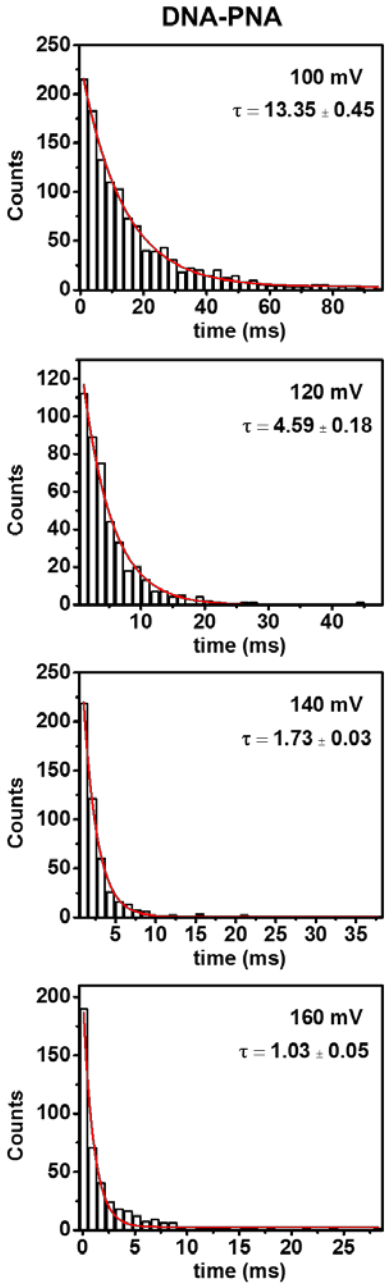

Figure SI14. Unzipping duration histograms as a function of voltage for the DNA-PNA duplexes. Data were recorded at 20 °C in 1 M KCl, 10 mM PBS, pH 7.4. An exponential decay was fit to the data to obtain the unzipping time. The *cis* side of the protein channel contained 8 μM of DNA-PNA sample.

15. Comparison of unzipping times of DNA-RNA duplexes with 3' and 5' overhangs.

In order to investigate if the orientation of the overhang influences the unzipping mechanism, we performed unzipping experiments using 5'-end poly C (24-nt) to compare with the 3'-end poly C (24-nt). The sequence used is given below.

DNA-RNA 5`-TCA TCA GTA GAA CTC AGA AAC $TCC_n$-3` n = 24

3`-AGU AGU CAU CUU GAG UCU UUG AG-5`

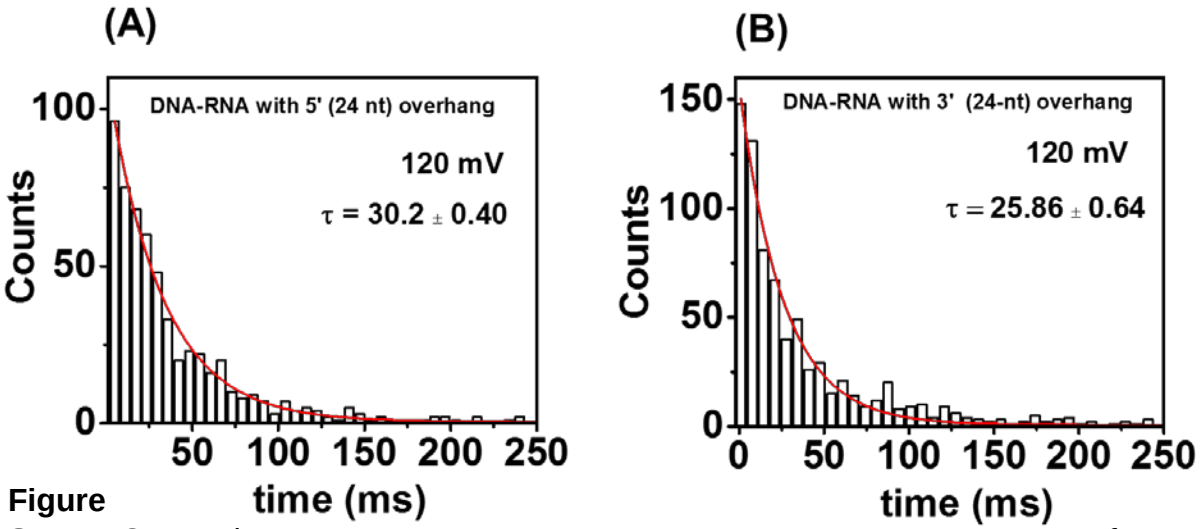

Figure SI15. Comparison of the unzipping duration histograms for the DNA-RNA duplexes. (*A*) 5' poly C overhang. (*B*) 3' poly C overhang. Data were recorded at 20 °C in 1 M KCl, 10 mM PBS, pH 7.4. An exponential decay was fit to the data to obtain the unzipping times. The *cis* side of the protein channel contained 8 μM of DNA-RNA in each case.